JOURNAL OF GEOPHYSICAL RESEARCH, VOL. 106, NO. A12, PAGES 28939–28948, DECEMBER 2001

Observation of the proton aurora with IMAGE FUV imager and simultaneous ion flux in situ measurements

J.-C. Gérard,[1] B. Hubert,[1] M. Meurant,[1] V. I. Shematovich,[2] D. V. Bisikalo,[2] H. Frey,[3] S. Mende,[3] G. R. Gladstone,[4] and C. W. Carlson[3]

Abstract. The far ultraviolet cameras on board the IMAGE satellite images the aurora in three different spectral regions. One of the channels of the spectrographic imager SI12 observes the Doppler-shifted Lyman α emission of precipitating protons. It makes it possible to spectrally discriminate between the proton and electron FUV aurora and to globally map the energetic protons. Its response depends on the auroral Lyman α line shape which reflects the characteristics of the proton pitch angle and energy distributions. We illustrate the dependence of the SI12 count rate on the characteristic energy of the proton precipitation and the viewing geometry. Simultaneous in situ observations of the precipitated protons have been collected during a FAST satellite pass when IMAGE was observing the global north polar region. The premidnight region located at the equatorward boundary of the oval is dominated by proton precipitation with a mean energy $\bar{E}$ = 7 keV which is separated from the electron component. The prenoon crossing exhibits a softer proton energy spectrum with $\bar{E}$ = 0.9 keV. The measured proton energy distribution is used as an input to a Monte Carlo model to calculate the expected SI12 signal along the magnetic footprint of the satellite orbit. If the different spatial resolution of the two types of measurements is accounted for, a good quantitative agreement is found with the IMAGE observations. Similarly, ion flux measurements collected on board the Defense Meteorological Satellite Program F15 satellite during an overflight in the postmidnight sector provide good agreement with the SI12 observations at the footprint aurora. The comparisons confirm the reliability of the FUV IMAGE cameras to remotely discriminate between the electron and the proton precipitations. The vertical emission rate profiles of the N_2 Lyman-Birge-Hopfield and O I (1356 Å) emissions are calculated in the proton-dominated premidnight region. It is shown that the protons and the electrons produce FUV emissions with contributions peaking at different altitudes. Excitation by secondary electrons dominates the production of both emissions.

1. Introduction

Auroral precipitations from the magnetosphere mainly consist of electrons and protons with a small fraction of other ions. As protons penetrate the atmosphere, they are progressively slowed down by elastic and inelastic collisions with major neutral constituents. During some of these collisions the proton captures an electron, leaving a fast hydrogen atom, possibly in an excited state. If the excited hydrogen atoms move toward the ground-based observer, the photon is emitted with a Doppler shift from the line center at rest. The observed line profile is the result of the integration of the contributions of all velocity vector projections on the line of sight. The spectral characteristics of its optical emission and its morphology were extensively studied from the ground as summarized by *Eather* [1967]. The ground neutral hydrogen (HI) auroral emissions are characterized by the presence of a broad wing extending to the blue, a less extended red wing, and a Doppler shift of the line peak. The magnetic zenith profiles for H_α and H_β peak at a Doppler shift corresponding to a field-aligned proton velocity of ~300 km s^{-1}. The blue wing (approaching H atoms for a ground-based observer) extends to ~2000 km s^{-1}. Little variation is observed in the line profile with the auroral brightness or latitude, except in the daytime polar cusp where narrower line profiles are usually observed [*Lorentzen et al.*, 1998].

The morphology of the proton aurora has been studied with instruments observing the weak hydrogen Balmer emissions, the only known signature detectable from the ground that can be unambiguously associated with proton precipitation. The electron and proton aurorae show distinct morphological features, although no global view of the proton aurora has been obtained so far. Systematic studies of proton aurora have been carried out using a chain of meridian spectrographs and photometers [*Montbriand*, 1971; *Vallance-Jones et al.*, 1982; *Samson et al.*, 1992] or airborne observations [*Eather and Mende*, 1971]. It was found that the proton aurora was usually accompanied by diffuse electron precipitation. A few attempts have been made to simultaneously measure the HI Balmer line profile from the ground and the precipitated proton energy spectrum. *Galperin et al.* [1976] compared in situ measurements of pitch angle distributions at different energies with auroral emission. *Soraas et al.* [1994] and *Synnes et al.* [1998] calculated the hydrogen line profiles for an arbitrary angle to the magnetic field. *Lorentzen et al.* [1998] used NOAA 12 satellite measurements of the incoming auroral proton fluxes to calculate the resulting H_α profile and compared it with ground-based observations in the dayside cusp region. They obtained a good match between the observed and calculated emission profiles.

[1]Laboratoire de Physique Atmosphérique et Planétaire, Université de Liège, Belgium.
[2]Institute of Astronomy, Russian Academy of Sciences, Moscow, Russia.
[3]Space Science Laboratory, University of California, Berkeley, California, USA.
[4]Southwest Research Institute, San Antonio, Texas, USA.

Paper number 2001JA900119.
0148-0227/01/2001JA900119$09.00

Hubert et al. [2001] calculated the distribution of the Lyman α (Ly α) and other FUV emission rates expected from the statistical ion precipitation distribution obtained by *Hardy et al.* [1989] from a large sample of proton measurements from DMSP satellites. They showed that the Ly α spatial distribution generally matches the ion precipitation pattern, although the efficiency of Ly α drops as the proton energy increases. *Gérard et al.* [2000] presented Ly α line profiles calculated with a direct Monte Carlo method and showed the importance of a stochastic treatment of the collisional angular scattering on the line profile.

Spacecraft-based observations of proton aurora were restricted to in situ satellite particle detection, and, until the launch of the Imager for Magnetopause-to-Aurora Global Exploration (IMAGE) satellite, no capability for remote sensing of the global proton aurora existed. Doppler-shifted auroral Ly α emission was observed by *Ishimoto et al.* [1989] using nadir FUV satellite spectroscopy. The line peaks were shifted toward longer wavelengths from the rest wavelength, and the line width was larger than the geocoronal midlatitude contribution. The inferred proton energy flux was consistent with statistical proton precipitation fluxes derived from satellite in situ observations. However, the proton-induced aurora had not been observed so far from a global perspective.

With the launch of the IMAGE satellite in March 2000, the FUV instrument fills this gap and provides the capabilities to simultaneously observe the aurora in three spectral bands: a broadband region extending from 1350 to 1700 Å (Wideband Imaging Camera(WIC)), a 50-Å passband centered on the O I (1356 Å) feature (SI13), and a narrow band system with a peak sensitivity at 1218 Å (SI12). Early results from the FUV were described by *Burch et al.* [2001], *Mende et al.* [2001], and *Frey et al.* [2001]. However, no quantitative comparison was made between in situ measurements of proton precipitation and the resulting SI12 observations.

In this study, we concentrate on the proton auroral spectrographic imager SI12. We first describe its sensitivity response to the characteristic of the incident proton beam. Next, we describe measurements comparing in situ ion measurements with parallel observations from IMAGE on the same magnetic field line. We then discuss the reliability and limitations of this new sensor to remotely sense proton precipitations.

2. Lyman α Line Profile and SI12 Response

The spectrographic imager SI12 is designed to measure the brightness of the Doppler-shifted Ly α auroral emission and monitor the global scale proton precipitation. The IMAGE SI12 has a grill system to reject the geocoronal Ly α emission at 1215.6 Å and allow a fraction of the broad auroral Ly α line profile [*Mende et al.*, 2000a, 2000b]. Since this emission is emitted by excited fast H atoms, the line profile for a given observation geometry depends on the energy spectrum of the incident auroral protons and their pitch angle distribution. In addition, the response of the SI12 instrument with its multiple passbands depends on the Ly α line profile. The shape of this profile is influenced by the orientation of the line of sight with respect to the magnetic field lines. Ideally, one would like to obtain a direct relationship between the observed instrumental count rate and the precipitated proton energy flux. However, the complexity of the atmospheric and instrumental processes involved make it necessary to simulate the SI12 response for a range of parameters describing the proton precipitation and the geometry of observations. The effects of the proton characteristic energy and pitch angle distribution were analyzed with a Monte Carlo direct simulation model.

2.1. Lyman α Model Calculations

The proton energy transport code is described in detail by *Gérard et al.* [2000]. It is based on the direct Monte Carlo method [*Shematovich et al.*, 1994; *Marov et al.*, 1997], which is a stochastic implementation of the solution of the Boltzmann equations for the H^+-H beam. In the thermosphere the protons exchange charge with the ambient constituents and generate a population of fast H atoms which, in turn, may be converted back to energetic protons. More specifically, the interactions of energetic protons H_f^+ with the main thermospheric constituents are described by the following processes:

$$H_f^+ + M \longrightarrow H_{f'}^+ + M^{(*)} \tag{1a}$$

$$H_f^+ + M \longrightarrow H_{f'}^+ + M^+ + e \tag{1b}$$

$$H_f^+ + M \longrightarrow H_{f'}^{(*)} + M^+, \tag{1c}$$

where M denotes N_2, O_2, or O.

These processes correspond to momentum and energy transfer in elastic and inelastic collisions (1a), ionization of target particles (1b), and charge transfer (1c). The fast hydrogen atoms H_f further interact with the atmosphere, transferring their momentum and kinetic energy by elastic and inelastic collisions, ionization, and stripping processes:

$$H_f + M \longrightarrow H_{f'}^{(*)} + M \tag{2a}$$

$$H_f + M \longrightarrow H_{f'}^{(*)} + M^+ + e \tag{2b}$$

$$H_f + M \longrightarrow H_{f'}^+ + M + e. \tag{2c}$$

A fraction of the $H_{f'}^{(*)}$ fast hydrogen atoms is produced in the H(2p) state by processes (1c), (2a), and (2b) and radiates Ly α photons. The Monte Carlo proton aurora code includes a detailed calculation of all collisional processes for both species and stochastically simulates the pitch angle redistribution of the simulated particles. These fast H atoms bear the signature of the proton characteristics before the electron-stripping collision. As excited H atoms move away from the down-viewing satellite, the Ly α photon is emitted with a Doppler shift to the red side of the unshifted line center. The observed line profile is the result of the integration of the contributions of all velocity vectors projected on the line of sight.

Simulations showed that the total line brightness is not simply proportional to the proton energy flux. The Ly α yield per unit precipitated energy flux drops as the characteristic proton energy increases [*Strickland et al.*, 1993; *Hubert et al.*, 2001]. The maximum Doppler red shift is 1.77 $\sqrt{E}$ Å, where E (in keV) is the initial proton energy. For a distributed energy spectrum the line shape depends on the spectral parameters describing the initial proton energy as discussed by *Gérard et al.* [2000]. Their study showed that the wavelength of the line peak, which corresponds to the most probable value of the velocity projection for the emitting atoms, is nearly independent of the characteristic energy above ~5 keV. The proton pitch angle distribution also plays a role, and field-aligned precipitation produces a narrower line profile than a hemispherically isotropic proton distribution. Finally, the orientation of the instrument is also important as the projection of the fast H atom velocity along the line of sight is different if observations are made along (parallel velocity) or perpendicular to the field lines (gyromotion).

2.2. SI12 Response to Lyman α Line Profile

We now examine how these factors affect the IMAGE FUV SI12 response to the auroral Ly α emission. Figure 1a shows the SI12 response curve together with the Ly α line shape calculated for a nadir observation of a proton aurora. In this example, the initial protons have a kappa energy distribution with a

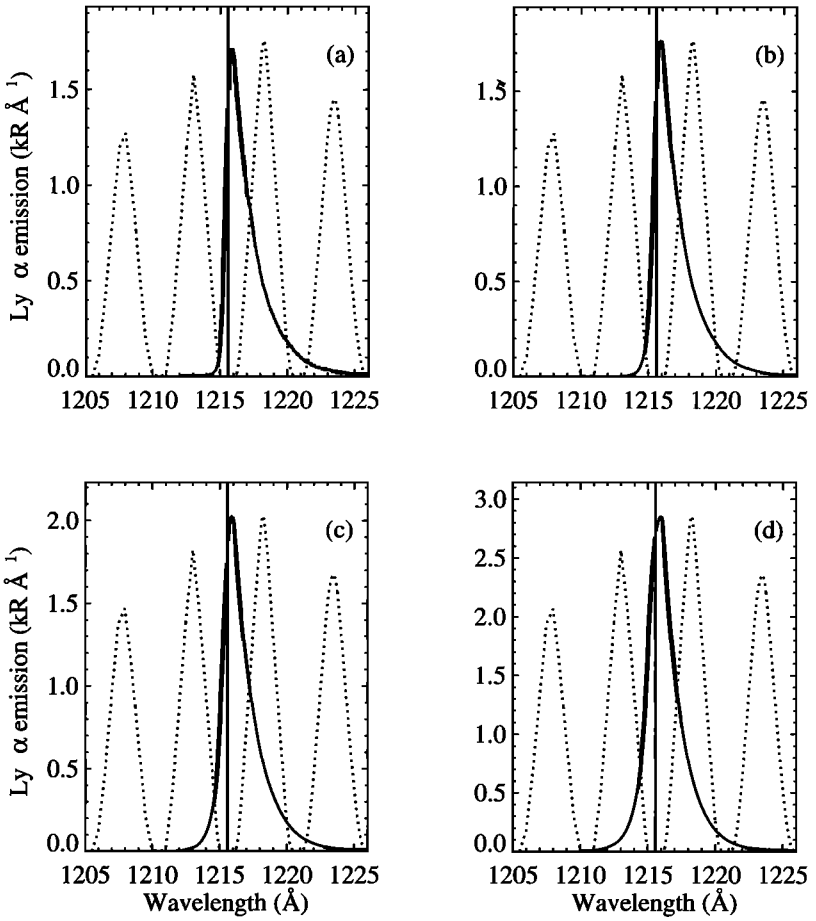

Figure 1. Calculated auroral Ly α line profile for an initial kappa proton distribution with E_0 = 2 keV and κ = 3.5 (solid line) for different view directions and a constant energy flux of 1 erg cm^{-2} s^{-1}: (a) view angle θ = 0° (along-field line), (b) θ = 20°, (c) θ = 40°, (d) θ = 60°. The shape of the SI12 response is also shown for comparison (dotted line).

characteristic energy E_0 = 2 keV and a κ index of 3.5 (average energy of 9.6 keV). The protons are injected assuming an isotropic pitch angle distribution. The blue-shifted component of the line profile is caused by upgoing fast H atoms. This upward moving population is due to protons that have reached their mirror point and to angular scattering of protons and fast H atoms [*Gérard et al.*, 2000]. The multiple SI12 spectral pass-band reflects the presence of the grill at the entrance of the Ly α spectral imager. At nadir (Figure 1a) the central peak at 1218 Å catches an appreciable fraction of the red-shifted Ly α photons, but the second peak at 1223.5 Å also contributes to the instrumental count rate by an amount dependent on the magnitude of the high-energy tail of the proton distribution. The secondary peak at 1213 Å transmits blue-shifted Ly α photons. The relative fraction of these three main contributions depends on the proton initial energy spectrum and the observation geometry. As the angle with the field line increases, the line profile is more symmetric and the two spectral windows on either side of the rest wavelength make nearly equal contributions. The SI12 count rate (per exposure) is also shown, based on the in-flight stellar calibration [*Gladstone et al.*, 2000]. The calculated integrated count rates are 6.6, 6.5, 6.2, and 5.8 counts pixel^{-1} kR^{-1} for lines of sight with an angle of 0°, 20°, 40°, and 60° at 110 km from the (assumed vertical) field line, respectively.

The response of the instrument observing a proton aurora in a given geometry has been simulated with the model described before. Figure 2 shows the efficiency of the Ly α emission rate as a function of the energy of incident monoenergetic protons. The drop in efficiency versus energy results from the increasing importance of other processes competing with excitation into the H(2*p*) state as the initial proton energy increases [*Strickland et al.*, 1993; *Gérard et al.*, 2000]. The emission rates are calculated for a nadir-viewing observation, assuming that the pixels are uniformly filled by the Ly α auroral emission. Table 1 lists the vertical emission rate and expected count rate calculated for three different proton energy distributions. The instrument efficiency drops for low-energy proton precipitation owing to the lack of an extended red-shifted Ly α wing. It is important to account for this effect when observing the daytime cusp aurora usually associated with low-energy proton precipitation. A 10% contribution relative to the 1218-Å instrumental peak corresponds to a 1-Å red shift, that is, 0.3 keV protons. Therefore protons with energy less than ~0.3 keV make negligible contribution in the SI12 instrument. This rapidly varying sensitivity at low energies also limits the accuracy of the signal conversion into energy flux units.

3. FAST-IMAGE Data Comparison

Simultaneous observations of in situ electron energy spectra and ground-based [*Frey et al.*, 1998] or space-borne cameras have been described using the Viking [*Kauristie et al.*, 1999] and Polar

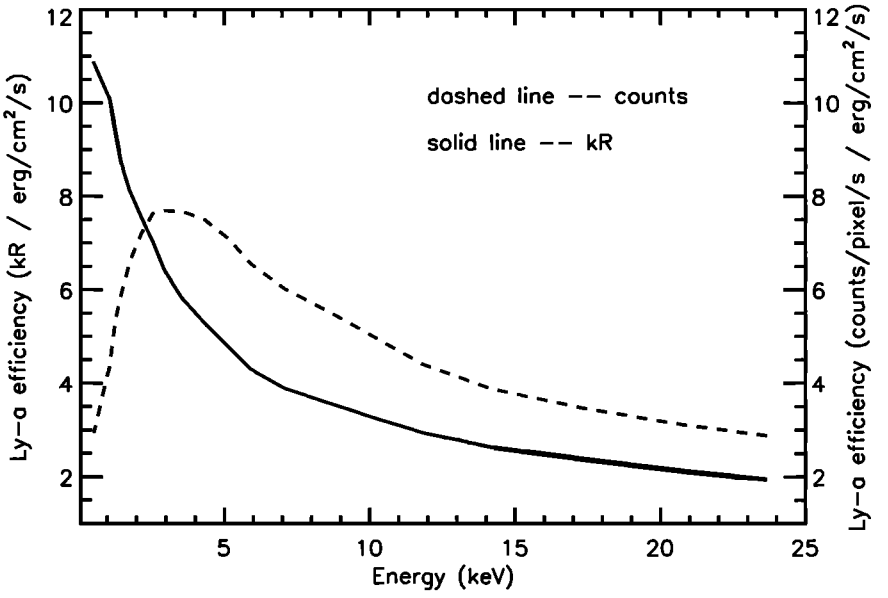

Figure 2. Calculated total Ly α nadir emission rate for a 1 erg cm^{-2} s^{-1} proton precipitation as a function of the proton initial energy (solid line). The corresponding SI12 count rate is also shown (dashed line).

[*Germany et al.*, 1997] ultraviolet cameras. Generally, the intensity variation along the satellite footprint extracted from the FUV images tracks reasonably well the variations of the precipitated energy, although differences are sometimes observed between the UV and particle oval boundaries. So far, no such comparison was possible for the proton aurora because of the lack of proton-sensitive FUV instruments in space.

Conjugate measurements with the IMAGE satellite offers for the first time the opportunity to compare the high time and energy resolution measurements of the auroral protons measured by FAST with the Ly α emission they induce at the footprint of the magnetic field lines. Some complications arise owing to (1) the diffuseness of the H^+-H glow in comparison with the high-altitude proton source region, (2) the smoothing effects of the FUV instrument, and (3) the different sampling times of the two sets of data.

3.1. FAST In Situ Particle Measurements

Electron and proton energy spectra measured on FAST orbit 15226 (June 24, 2000) at ~4000 km between 06:10 and 06:50 UT are used for this study. The magnetic local times (MLT) of the auroral crossings are close to 22:00 and 09:25 MLT. This orbit was selected because the FAST electrostatic analyzers (ESAs) measured a substantial flux of ions at the equatorward boundary of the auroral oval. In addition, little temporal variation was observed during the period used for this study. The four FAST ESAs probe all pitch angles in the spacecraft spin plane. The measured energy range is 4 eV to 30 keV for electrons and 3 eV to 25 keV for ions [*Carlson et al.*, 1998]. The spacecraft altitude is close to 4000 km. We use 5-s average energy spectra.

Table 1. Calculated Vertical Emission Rate and SI12 Count Rate for a 1 erg cm^{-1} s^{-1} Proton Precipitation (kappa Distribution)

Mean Energy, keV	Nadir Emission Rate, kR	SI12 Count Rate, counts $pixel^{-1}$
2	9.0	36
8	4.8	30
25	2.4	17

Frey et al. [2001, Figure 1] shows the SI 12 image, the footprint of the FAST orbital track at 100 km, and the mapped position of FAST at 0622:20 UT. At this time the spacecraft had left the region of maximum ion precipitation but was in an area of intense downward electron flux.

Figure 3 shows the electron and ion energy fluxes measured in the loss cone during the sequence of nightside oval, polar cap, and daytime oval crossings. The nightside auroral region is clearly identified by its signature in the electron energy flux. The total electron fluxes reaches ~13 erg cm^{-2} s^{-1} near the poleward boundary of the nightside oval. It drops by more than 3 orders of magnitude in the polar cap and reaches a peak of 6 erg cm^{-2} s^{-1} in the morning oval. The ion fluxes are more modest with a peak value of 2.6 erg cm^{-2} s^{-1} at 0617:30 UT located equatorward of the intense electron precipitation. In the morning proton oval, values remain below 1 erg cm^{-2} s^{-1}. We note that the equatorward shift of the peak of the proton precipitation on the nightside is consistent with ground-based observations of the hydrogen Balmer emissions, indicating the frequent presence of an auroral region dominated by protons equatorward of the main electron-excited arcs in the premidnight sector. The expected Ly α distribution was recently described by *Hubert et al.* [2001] on the basis of the statistical precipitation ion pattern by *Hardy et al.* [1989].

In spite of the absence of time variation, the energy spectra measured in the oval showed substantial spatial variations along the satellite orbit. Figure 4 shows examples of two proton energy spectra measured above 10 eV at 0618 and 0642 UT, that is, at the peaks of the nightside and dayside proton crossings, respectively. The two spectra show distinct features. The nighttime spectrum is characterized by a total flux of 0.16 erg cm^{-2} s^{-1} and a mean ion energy of 7 keV. It shows a quasi-continuous decrease from 0.3 to 1.5 keV followed by a less pronounced peak at 6 keV. The dayside spectrum is nearly Maxwellian above 100 eV with a peak at 350 eV. The corresponding total flux is 0.11 erg cm^{-2} s^{-1} with a mean energy of 0.9 keV. The prenoon spectrum is thus typical of a fairly cold ion population, whereas the premidnight spectrum bears the signature of an acceleration mechanism providing a high-energy component. The segment of FAST proton data is used as an input to the Monte Carlo code to calculate the emerging Ly α line shape and brightness and the expected SI12 count rate. It is then compared with the observations made from 7 R_E by the SI12

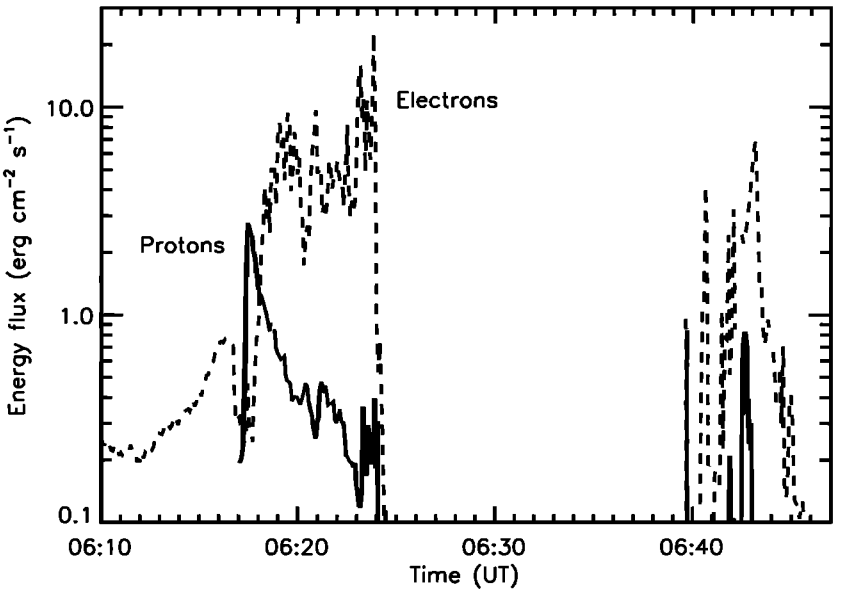

Figure 3. Time variation of the electron and proton energy fluxes measured by the detectors on board the FAST satellite on orbit 15226.

imager. As an example, Figure 5 shows the line profile calculated at 0618 UT. The profile shows similar features to those calculated for analytical distributions in Figure 1. No red-shifted wing is predicted above 1225.4 Å, reflecting the 30-keV cutoff of the FAST detectors.

3.2. Comparison With IMAGE FUV

The images obtained with the WIC and SI instruments at 0622:20 UT were presented by *Frey et al.* [2001, Figure 2]. We extracted the instrumental count rate for the SI12 pixel corresponding to the footprint of the magnetic field line at the instantaneous spacecraft position. A SI12 Doppler-shifted Ly α image is obtained every 2 min. During this time the FAST spacecraft moved by ~700 km along its orbit. Therefore out of each individual FUV image the SI12 count rate was extracted along the footprint track of FAST from the position 1 min before to 1 min after the central snapshot time. A continuous Ly α brightness sequence is thus produced from 20 individual SI12 images. This time sequence is shown in Figure 6. The bright signal in the SI12 camera in the premidnight aurora is shifted equatorward of the peak of the WIC (N_2 Lyman-Birge-Hopfield (LBH)) and SI13 (O I (1356 Å) plus LBH) maxima. This is a clear indication that the SI12 channel is not sensitive to electron-excited spectral components. The time period used for this study was characterized by fairly stable auroral conditions, as evidenced by images in all three cameras.

Comparison between the FAST data and the FUV observations requires some averaging of the FAST data points. The amount of smoothing for a given FUV frame depends on the radial distance of the spacecraft, the view angle from nadir, and the instrumental

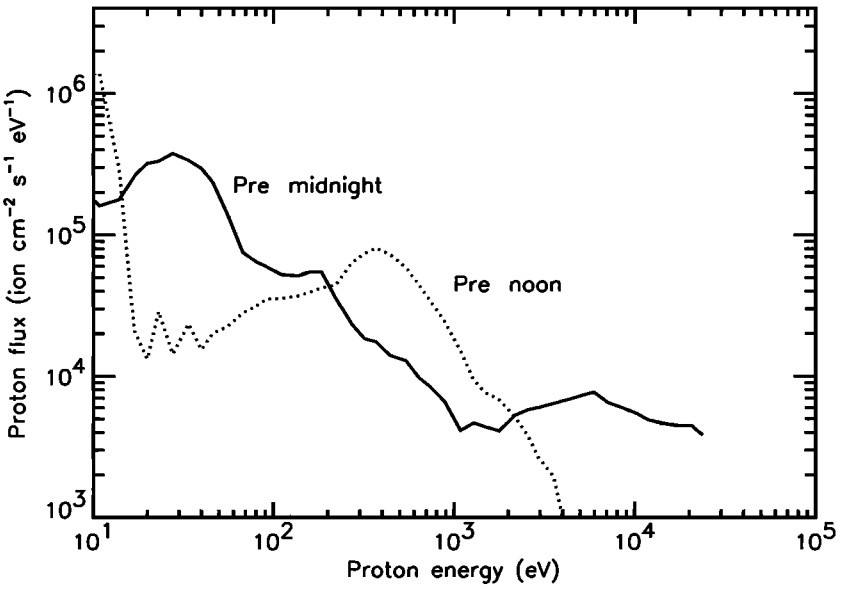

Figure 4. Proton energy spectra measured at 0617:32 and 0642:04 UT by FAST on orbit 15226.

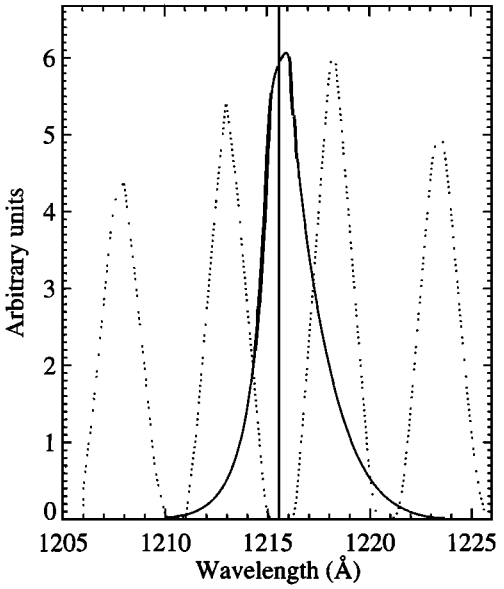

Figure 5. Ly α line profile calculated to simulate an IMAGE SI12 observation at 0617:32 UT on the basis of the ion energy spectrum measured by the FAST satellite.

point spread function, including the important effect of the time delay integration (TDI) setting. The proton aurora is spread over a geographic area exceeding the proton precipitation region. As protons interact with the atmosphere, they undergo charge-exchange collisions (process (1c)), and the magnetically unconstrained fast H atoms may travel some distance across the field lines. This process results in the spreading of an initially confined beam and will therefore contribute to redistribute spatially the surface brightness. Consequently, the Ly α emission is not expected to follow the morphology of the proton source to the same detail as the N_2 LBH or O I (1356 Å) emissions reflect the electron precipitation [*Eather*, 1967]. This dilution effect was modeled by *Davidson* [1965] using a Monte Carlo method. The calculated emission falls to 10% of the peak value at ~2° of latitude each side of the field line of the initial injection. More recently, *Kozelov and Ivanov* [1992] investigated the H^+-H beam spreading with a Monte Carlo model. They showed that the radius of the beam encircling 80% of the energy flux strongly varies with altitude and maximizes above the altitude of maximum energy deposition. It is typically 100–150 km wide for 1–10 keV protons. In a one-dimensional approach, emission rates are calculated for each proton energy spectrum measured by FAST. A slant column integration is performed for the actual view angle, neglecting latitudinal gradients in the integration ("airglow" approximation). This approximation is valid if the horizontal path through the effective emission layer is small in comparison with the characteristic horizontal scale of the brightness variations. This assumption may not be valid for the highly structured electron aurora. It is crudely satisfied for the more diffuse Ly α aurora.

The width of the point spread function (PSF) was determined from the shape of hot star images observed during a sky survey after these observations. It is on the order of 3 SI12 pixels in the spin direction and 1–2 pixels across. The PSF combines the response of the instrument optics and the residual effects of the TDI system. Another source of uncertainty is the fact that the SI12 signal in each pixel includes emission from adjacent lateral regions not probed by the FAST detector. Adopting an instrumental resolution of 3 SI12 pixels and a beam spreading of 100 km, we use an effective width of 340 km at nadir and 740 km at 60° from nadir. These distances project into an orbital motion of 96 and 170 s, respectively, of the FAST satellite.

The results in Figure 6 indicate that the modeled Ly α emission rate agrees well in magnitude with the observations. However, the width of the Ly α oval emission exceeds that of the proton precipitation region mapped down from FAST along the magnetic field lines. Although this difference of spatial extent may be due to the diffuseness of the proton-H atom beam, it may also be caused by other factors linked to the mapping procedure as discussed in section 4. Finally, high-energy protons above the 30-keV FAST detector limit may also contribute to the Ly α emission rate. They

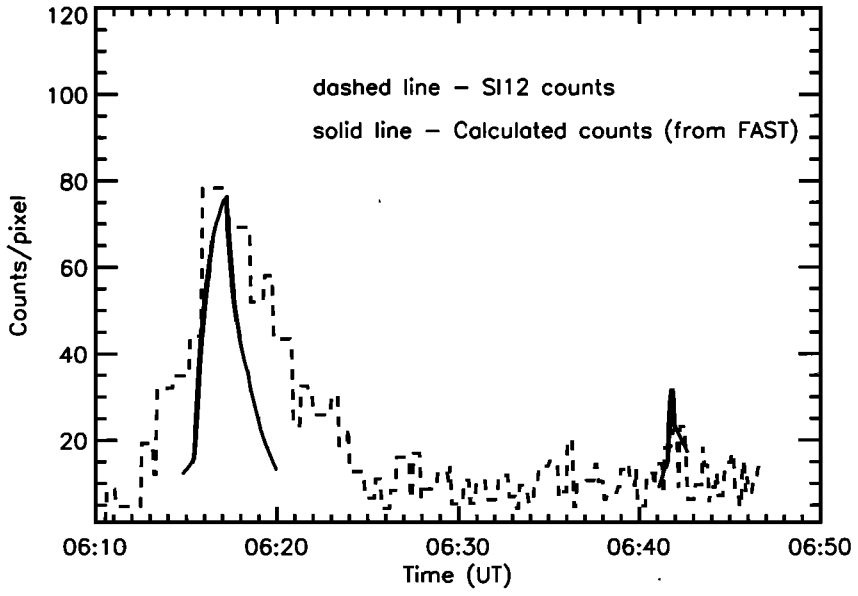

Figure 6. Comparison of the simulated SI12 count rate based on the FAST proton energy spectra (solid line) with the corresponding SI12 signal (dotted line). The calculated Ly α signal has been smoothed to account for the instrumental point spread function and proton beam spreading (see text).

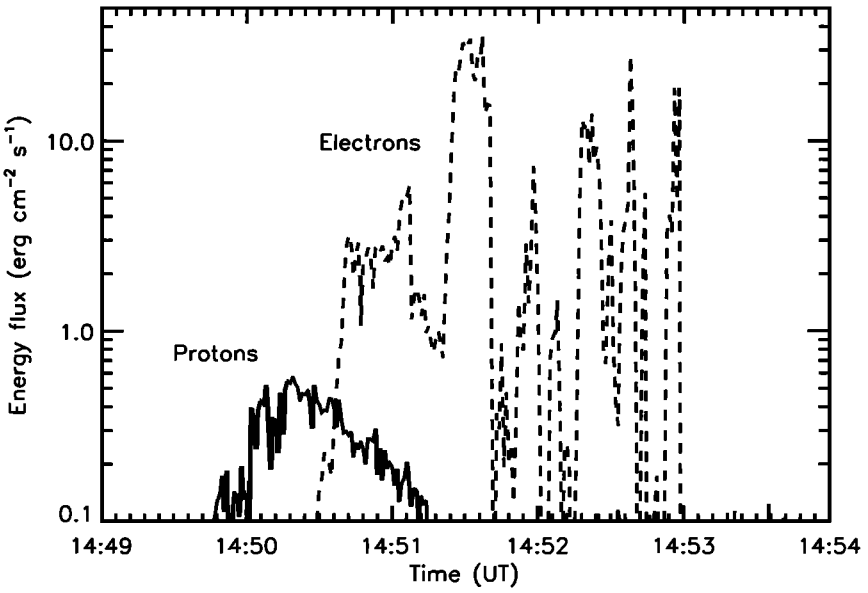

Figure 7. Time variation of the electron and proton energy fluxes measured by the detectors on board the DMSP F15 satellite on December 3, 2000.

were not accounted for in these simulations. As may be deduced from the shape of the proton spectra, a fraction of the proton energy flux between 0617 and 0618 UT has been underestimated during this period. The Ly α calculated intensity is therefore a lower limit during this time period.

4. DMSP-IMAGE Comparison

As an independent check of the consistency between in situ ion measurements and SI12 images, we analyzed parallel observations during a Defense Meteorological Satellite Program (DMSP) satellite crossing of the premidnight oval. The measurements were made with the DMSP F15 satellite on December 3, 2000, as the spacecraft was crossing the nightside auroral oval from 1449:35 to 1453:00 UT. The DMSP satellites are quasi-polar sun-synchronous satellites at a nominal altitude of 830 km with an orbital period of ~100 min. DMSP F15 carries the SSJ/4 auroral particle spectrometers which measure the electron and ion particle fluxes between 30 eV and 30 keV. The detectors are oriented toward the zenith and produce a complete spectrogram in the loss cone every second, but 5-s averages are used in this study. The DMSP detectors provide energy spectra of electrons and ions every second in 20 logarithmically spaced energy channels extending from 20 eV to 20 keV. Figure 7 shows the variation of the electron and proton energy fluxes along the spacecraft orbit. The electron flux reaches 35 ergs cm^{-2} s^{-1} at 1451:35 UT. The maximum proton energy flux of ~0.6 erg cm^{-2} s^{-1} occurred at 1450:20 UT, that is, ~75 s before

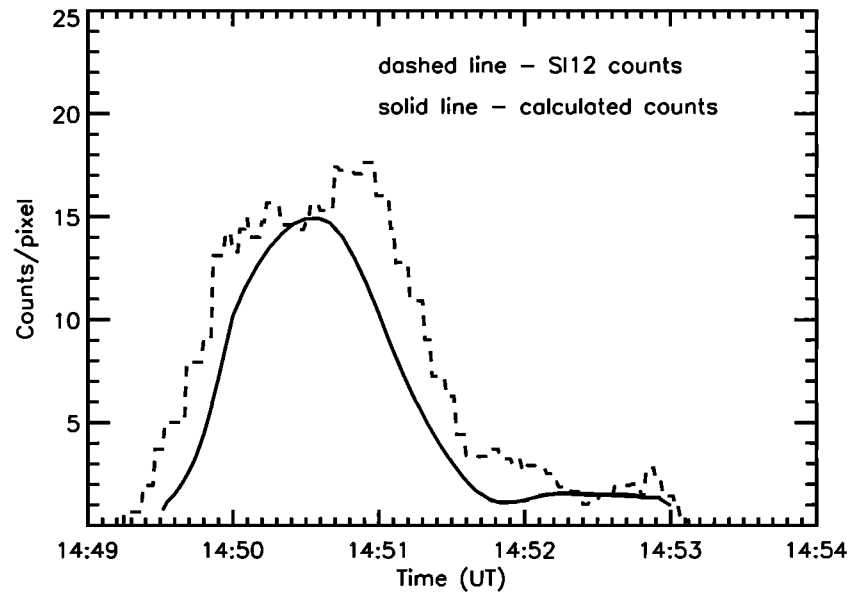

Figure 8. Comparison of the simulated smoothed SI12 count rate based on the DMSP F15 proton energy spectra (solid line) with the corresponding SI12 signal (dashed line).

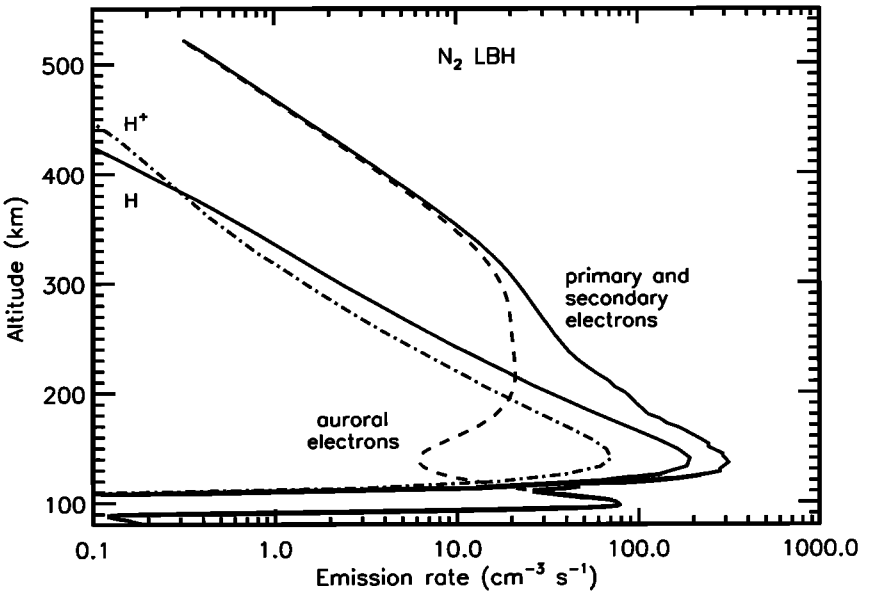

Figure 9. Vertical distribution of the N_2 Lyman-Birge-Hopfield bands calculated using FAST measurement of the electron and proton energy spectra for orbit 15226 at 0617:32 UT: direct excitation by the H^+ and H beams (dashed-dotted lines), auroral electrons (dashed line), and auroral and secondary (from p-H ionization) electrons (solid line).

the electron flux peak. This maximum is located at 64°N magnetic latitude (MLAT) and 20:40 MLT. A secondary peak less than ~0.1 erg cm^{-2} s^{-1} observed at 1452:40 UT, poleward of the maximum electron energy precipitation, is not seen in Figure 7. A substantial fraction of the proton energy is deposited equatorward of the electron auroral precipitation.

Figure 8 shows the intensity variation along the DMSP satellite footprint extracted from the SI12 images between 1449 and 1454 UT following the procedure described before. For comparison, the predicted SI12 count rate is also shown, following smoothing over 100 s. The overall agreement between the calculated and observed count rate is excellent. The model calculation of the SI12 signal shows a peak at 1450:55 UT, ~24 s after (and 0.3° poleward of) the calculated maximum count rate. The ion energy spectra indicate that from 1449:40 to 1450:40 UT the proton average energy exceeded 15 keV, and a fraction of the proton energy flux was carried by protons with energies in excess of the 20-keV detector limit. However, as seen in Figure 2, the efficiency of these high-energy protons makes only a relatively small contribution to the observed SI12 count rate. It was not accounted for here.

5. Other FUV Emissions

The auroral ionosphere is usually submitted to both electron and proton bombardment. Previous theoretical work has described the combined effect of electron and proton precipitation on FUV emissions [*Strickland et al.*, 1993; *Hubert et al.*, 2001]. However

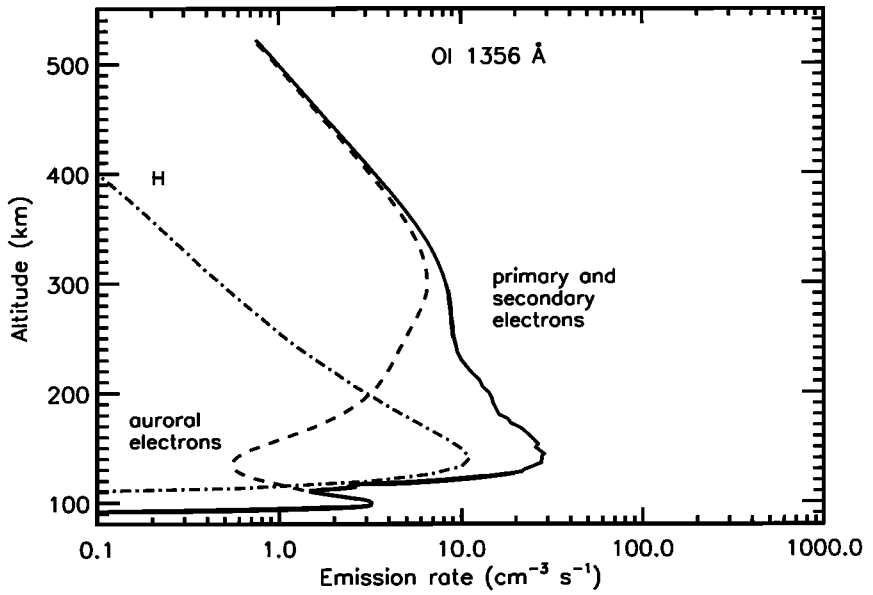

Figure 10. Same as Figure 9 for the O I (1356 Å) emission.

these simulations were based on theoretical energy flux distributions derived from statistical particle precipitation models. These calculations showed that at certain local times and latitudes, FUV emissions may be predominantly excited by protons. We use the simultaneously measured energy spectra of both electrons and protons to illustrate this important point. The FAST measurements along orbit 15226 described in section 3.1 indicate that protons dominate the total energy flux at the equatorward boundary of the premidnight oval (Figure 3).

We examine the production of two important FUV emissions also measured with the IMAGE satellite: the N_2 LBH bands and the O I (1356 Å) at 0618 UT, the time of the highest proton energy flux precipitation. Figure 9 shows the vertical distribution of the LBH production rate by primary auroral electrons, proton impact, and fast H atom impact. The primary electrons produce a double-peaked emission rate distribution with a first maximum at 200 km, associated with the soft electron component and the main peak at 98 km due to the higher-energy component. The direct contribution of the H^+ and H impact shows a single peak at 138 km associated with the quasi Maxwellian proton energy distribution measured by FAST (Figure 4). The total excitation rate includes the contributions of the primary auroral electrons, the H^+ and H components, and the secondary electrons generated by the proton and H atom ionizing collisions. Figure 9 shows that at the main peak the LBH excitation is dominated by the proton precipitation. More specifically, the secondary electrons due to ionization by $H\text{-}H^+$ dominate the direct proton contribution which, in turn, exceeds the primary electrons component. Similar conclusions for the O I (1356 Å) may be drawn from Figure 10. The main peak at 140 km is dominated by the contribution of the secondary electrons produced by ionization due to proton impact. No direct contribution from collision with protons are included owing to the lack of experimental cross section.

6. Discussion and Conclusions

The agreement between the calculated Ly α emission rate and the SI12 observations may be considered as quite good, considering all sources of uncertainties and errors. These include calibrations of both the SI12 camera and the FAST or DMSP detectors, mapping of the footprint of the magnetic field lines using the International Geomagnetic Reference Field model, and the spacecraft pointing information, uncertainties in the model cross sections and in the Mass Spectrometer Incoherent Scatter atmospheric model. High-energy protons above the 30-keV limit of the detectors on both satellites may also add to the Ly α high-energy line wing and to the SI12 count rate. In addition, it is assumed that no process affects the proton isotropy in the loss cone and the proton energy distribution between the FAST orbit and the region of Ly α emission, that is, ~4000 km lower.

As mentioned in section 3.2, our one-dimensional approach also limits the accuracy of evaluation of the beam spreading width and the line of sight integration. Nevertheless, the agreement obtained in this comparison validates our modeling approach and the instrument calibration. It also confirms the efficiency of the SI12 imager on board IMAGE to remotely probe the proton aurora in a quantitative way. The differences in widths between the proton and the Ly α premidnight ovals may stem from instrumental or physical reasons. The particle detectors sample a very small volume in comparison with the size of the point spread function of the Ly α camera observing near IMAGE apogee. Also, the detectors sample only along the orbital track, whereas SI12 integrated over a two-dimensional area including structures perpendicular to the orbit and thus not observed by FAST or DMSP. Finally, the lateral spreading of the fast H atoms may exceed the values used for our smoothing function. A physical process affecting the proton precipitation in the ionosphere between 4000 and 150 km cannot be excluded. Upward field-aligned currents have been associated with downstreaming fluxes of protons which accelerate the ionospheric protons below the FAST satellite at 4000 km.

We also confirm, on the basis of the two data sets, that the proton aurora, which is frequently observed equatorward of the premidnight electron aurora, produces oxygen and N_2 FUV emissions in excess of the electron component. It is shown that a complex vertical distribution of emission rate may result from the combined electron-proton precipitation. The existence of double-peaked structures as described in section 5 clearly complicates the FUV remote-sensing analysis in the absence of simultaneous particle measurements. In this case, uncertainties in the conversion of instrumental signals into proton precipitated fluxes may be evaluated on the basis of the table and figures given in this study.

The direct comparison between in situ proton fluxes and SI12 was discussed in detail in this study. However, the inverse problem of the determination of the proton flux properties from FUV observations is more complex. The Doppler-shifted Ly α line is the only clear signature of energetic proton precipitation. The auroral protons and their cascades of secondary electrons excite other FUV emissions, excluding the N_2 Lyman-Birge-Hopfield and the O I (1356 Å) features. These emissions are imaged synchronously with SI12 by the WIC and SI13 cameras, respectively. However, the three simultaneous images cannot provide the four unknown quantities ϕ_e, $\bar{E}_e$, ϕ_p and $\bar{E}_p$ (total energy fluxes and average energies of electrons and protons, respectively) and an assumption has to be made on one of them. Protons generally make smaller contributions than electrons [*Hardy et al.*, 1989]. Therefore a reasonable guess is generally made on the average proton energy. Use of Table 1 and Figure 2 makes it then possible to calculate ϕ_p and to subtract the proton contribution from the WIC and SI13 signals. It is thus generally not possible to determine the proton characteristic energy except in regions dominated by auroral proton precipitation.

Acknowledgments. J. C. G. is supported by the Belgian National Fund for Scientific Research (FNRS). This work was funded by the PRODEX program of the European Space Agency (ESA), the Belgian Fund for Collective Fundamental Research (grant FRFC 97-2.4569.97), and the Russian Foundation for Basic Research (RFBR grant 99-02-17620).

Hiroshi Matsumoto thanks M. Nakamura and R. Fujii for their assistance in evaluating this paper.

References

Burch, J. L., et al., Views of Earth's magnetosphere with the IMAGE satellite, *Science*, *291*, 619, 2001.

Carlson, C. W., R. F. Pfaff, and J. G. Watszın, The Fast Auroral Snapshot (FAST) mission, *Geophys. Res. Lett.*, *25*, 2013, 1998.

Davidson, G. T., Expected spatial distribution of low-energy protons precipitated in the auroral zone, *J. Geophys. Res.*, *70*, 1061, 1965.

Eather, R. H., Auroral proton precipitation and hydrogen emissions, *Rev Geophys.*, *5*, 207, 1967.

Eather, R. H., and S. B. Mende, Airborne observations of auroral precipitation patterns, *J. Geophys. Res.*, *76*, 1746, 1971.

Frey, H. U., G. Haerendel, J. H. Clemmons, M. H. Boehm, J. Vogt, O. H. Bauer, D. D. Wallis, L. Blomberg, and H. Lühr, Freja and ground-based analysis of inverted-V events, *J. Geophys. Res.*, *103*, 4303, 1998.

Frey, H. U., S. B. Mende, C. W. Carlson, J.-C. Gérard, B. Hubert, J. Spann, R. Gladstone, and T. J. Immel, The electron and proton aurora as seen by IMAGE FUV and FAST, *Geophys. Res. Lett.*, *28*, 1135, 2001.

Galperin, Y. I., R. A. Kovrazhkin, Y. N. Ponomarev, J. Crasnier, and J. A. Sadaud, Pitch angle distribution of auroral protons, *Ann Geophys.*, *32*, 109, 1976.

Germany, G. A., G. K. Parks, M. Brittnacher, J. Cumnock, D. Lummerzheim, J. F. Spann, L. Chen, P. G. Richards, and F. J. Rich, Remote determination of auroral energy characteristics during substorm activity, *Geophys. Res. Lett.*, *24*, 995, 1997.

Gérard, J. C., B. Hubert, D. V. Bisikalo, and V. I. Shematovich, A model of the Lyman α line profile in the proton aurora, *J. Geophys Res.*, *105*, 15,795, 2000.

Gladstone, R. G., et al., Stellar calibration of the WIC and SI imagers and the GEO photometer on IMAGE/FUV, *Eos Trans. AGU*, *81*(48), SM72A-06, 2000.

Hardy, D. A., M. S. Gussenhoven, and D. Brautigam, A statistical model of auroral ion precipitation, *J. Geophys. Res.*, *94*, 370, 1989.

Hubert, B., J.-C. Gérard, D. V. Bisikalo, V. I. Shematovich, and S. C. Solomon, The role of proton precipitation in the excitation of auroral FUV emissions, *J. Geophys. Res.*, *106*, 2001.

Ishimoto, M., C. I. Meng, G. R. Romick, and R. E. Huffman, Doppler shift of auroral Lyman α observed from a satellite, *Geophys. Res. Lett.*, *16*, 143, 1989.

Kauristie, K., J. Weygand, T. I. Pulkkinen, J. S. Murphree, and P. T. Newell, Size of the auroral oval: UV ovals and precipitation boundaries compared, *J. Geophys. Res.*, *104*, 2321, 1999.

Kozelov, B. V., and V. E. Ivanov, Monte-Carlo calculation of proton-hydrogen atom transport in N_2, *Planet. Space Sci.*, *40*, 1503, 1992.

Lorentzen, D. A., F. Sigernes, and C. S. Deehr, Modeling and observations of dayside auroral hydrogen emission Doppler profiles, *J. Geophys. Res.*, *103*, 17,479, 1998.

Marov, M. Y., V. I. Shematovich, D. V. Bisikalo, and J.-C. Gérard, *Nonequilibrium Processes in Planetary and Cometary Atmospheres: Theory and Applications*, Kluwer Acad., Norwell, Mass., 1997.

Mende, S. B., et al., Far ultraviolet imaging from the IMAGE spacecraft, 1, System design, *Space Sci. Rev.*, *91*, 243, 2000a.

Mende, S. B., et al., Far ultraviolet imaging from the IMAGE spacecraft, 3, Spectral imaging of Lyman alpha and OI 135.6 nm, *Space Sci. Rev.*, *91*, 287, 2000b.

Mende, S. B., H. U. Frey, M. Lampton, J.-C. Gérard, B. Hubert, S. Fuselier, G. R. Gladstone, and J. L. Burch, Global observations of proton and electron auroras in a substorm, *Geophys. Res. Lett.*, *28*, 1139, 2001.

Montbriand, L. E., The proton aurora and auroral substorm, in *Radiating Atmosphere*, edited by B. M. McCormac, p. 366, D. Reidel, Norwell, Mass., 1971.

Samson, J. C., L. R. Lyon, P. T. Newell, F. Creutzberg, and B. Xu, Proton aurora and substorm intensification, *Geophys. Res. Lett.*, *19*, 2167, 1992.

Shematovich, V. I., D. V. Bisikalo, and J.-C. Gérard, A kinetic model of the formation of the hot oxygen geocorona, 1, Quiet geomagnetic conditions, *J. Geophys. Res.*, *99*, 217, 1994.

Soraas, F., K. Maseide, P. Turheim, and K. Aarsnes, Doppler-shifted auroral H_β emission: A comparison between observations and calculation, *Ann Geophys.*, *12*, 1052, 1994.

Strickland, D. J., R. E. Daniell, Jr., J. R. Jasperse, and B. Basu, Transport-theoretic model for the electron-proton-hydrogen atom aurora, 2, Model results, *J. Geophys. Res.*, *98*, 21,533, 1993.

Synnes, S. A., F. Soraas, and J. P. Hansen, Monte-Carlo simulations of proton aurora, *J. Atmos. Sol.-Terr. Phys.*, *60*, 1695, 1998.

Vallance-Jones, A., F. Creutzberg, R. L. Gattinger, and F. A. Harris, Auroral studies with a chain of meridian scanning photometers, 1, Observations of proton and electron aurora in magnetospheric substorms, *J. Geophys. Res.*, *87*, 4489, 1982.

D. V. Bisikalo and V. I. Shematovich, Institute of Astronomy, Russian Academy of Sciences, 48 Pjatnistkaja Street, Moscow, Russia. (bisikalo@inasan.rssi.ru, shematov@inasan.rssi.ru)

C. W. Carlson, H. Frey, and S. Mende, Space Sciences Laboratory, University of California, Centennial Drive at Grizzly Peak Boulevard, Berkeley, CA 94720-7450, USA. (carlson@ssl.berkeley.edu; hfrey@ssl.berkeley.edu; mende@ssl.berkeley.edu)

J.-C. Gérard, B. Hubert, and M. Meurant, Laboratoire de Physique Atmosphérique et Planétaire, Institut d'Astrophysique et de Géophysique, 5 avenue de Cointe, B-4000 Liège, Belgium. (gerard@astro.ulg.ac.be; hubert@astro.ulg.ac.be)

G. R. Gladstone, Southwest Research Institute, 6220 Culebra Road, San Antonio, TX 78228-0510, USA. (randy@whistler.space.swri.edu)

(Received March 3, 2001; revised August 9, 2001;
accepted August 9, 2001.)